Effects of Target Corrosion on Advanced EMI Signatures in Underwater Environments

Final Report

SERDP Project MR-2500

Daniel Steinhurst, Glenn Harbaugh (Nova Research)

Matthew Strom (NRL, Code 6130)

Joseph Bucaro (NRL, Code 7130)

Thomas Bell (Leidos Corporation)

Bruce Barrow (Acorn SI)

June, 2017

Page Intentionally Left Blank

REPORT DOCUMENTATION PAGE

Form Approved
OMB No. 0704-0188

The public reporting burden for this collection of information is estimated to average 1 hour per response, including the time for reviewing instructions, searching existing data sources, gathering and maintaining the data needed, and completing and reviewing the collection of information. Send comments regarding this burden estimate or any other aspect of this collection of information, including suggestions for reducing the burden, to the Department of Defense, Executive Services and Communications Directorate (0704-0188). Respondents should be aware that notwithstanding any other provision of law, no person shall be subject to any penalty for failing to comply with a collection of information if it does not display a currently valid OMB control number.
PLEASE DO NOT RETURN YOUR FORM TO THE ABOVE ORGANIZATION.

1. REPORT DATE *(DD-MM-YYYY)*	2. REPORT TYPE	3. DATES COVERED *(From - To)*
30-10-2017	SERDP Final Report	02/19/2015 - 09/30/2016

4. TITLE AND SUBTITLE
Effects of Target Corrosion on Advanced EMI Signatures in Underwater Environments (non-Acoustic)
Final Report
SERDP Project MR-2500

5a. CONTRACT NUMBER
N00173-14-D-2013

5b. GRANT NUMBER

5c. PROGRAM ELEMENT NUMBER
0603716D8Z

6. AUTHOR(S)
D.A. Steinhurst[1], G.R. Harbaugh[1], M.J. Strom[2], J.A. Bucaro[3], T.H. Bell[4], B.J. Barrow[5]

5d. PROJECT NUMBER
MR-2500

5e. TASK NUMBER

5f. WORK UNIT NUMBER
61-5802

7. PERFORMING ORGANIZATION NAME(S) AND ADDRESS(ES)
[1]Nova Research, Inc., 1900 Elkin St., Ste 230, Alexandria, VA 22308;
[2]NRL Code 6130; [3]Excet, Inc., 6225 Brandon Ave., Ste 360, Springfield, VA 22150;
[4]Leidos, Arlington, VA; [5]Acorn SI, 2928 S. Buchanan St., Ste C-1, Arlington, VA 22206

8. PERFORMING ORGANIZATION REPORT NUMBER
MR-2500

9. SPONSORING/MONITORING AGENCY NAME(S) AND ADDRESS(ES)
Strategic Environmental Research and Development Program (SERDP) Program Office
4800 Mark Center Drive, Suite 17D08
Alexandria, VA 22350-3605

10. SPONSOR/MONITOR'S ACRONYM(S)
SERDP

11. SPONSOR/MONITOR'S REPORT NUMBER(S)
MR-2500

12. DISTRIBUTION/AVAILABILITY STATEMENT
Approved for public release; distribution unlimited.

13. SUPPLEMENTARY NOTES

14. ABSTRACT
Munitions submerged in sea or fresh water for any length of time may become heavily rusted or encrusted with sea growth. At present there is very little hard empirical data on the effects of corrosion and biofouling in marine environments on the electromagnetic induction (EMI) and physical acoustic response signatures of military munitions. This research systematically examined the effects of two primary types of corrosion and biofouling that are commonly found in the underwater environment. A combination of laboratory tank tests and controlled exposure in real-world underwater environments were used. No measurable difference was seen between the EMI response of bare surrogates and those with the corrosion layers applied. We conclude without specifically demonstrating it that there would be little impact on acoustic detection ranges, classification performance, or maximum burial depth caused by a thin corrosion layer.

15. SUBJECT TERMS
Corrosion, Underwater, Salt Water, Classification, Unexploded Ordnance (UXO), Multi-sensor Towed Array Detection System (MTADS), Electromagnetic Induction (EMI), EMI response, transient electromagnetic induction (TEM), TEMTADS

16. SECURITY CLASSIFICATION OF:			17. LIMITATION OF ABSTRACT	18. NUMBER OF PAGES	19a. NAME OF RESPONSIBLE PERSON
a. REPORT	b. ABSTRACT	c. THIS PAGE			J.N. Russell, NRL, Code 6170
Unclassified	Unclassified	Unclassified	Unlimited	33	19b. TELEPHONE NUMBER *(Include area code)* (202) 767-5879

Reset

Standard Form 298 (Rev. 8/98)
Prescribed by ANSI Std. Z39.18

Page Intentionally Left Blank

Abstract

The effects of corrosion and biofouling on the electromagnetic induction (EMI) and physical acoustic response signatures of military munitions located at underwater munitions response sites are relatively unknown at this time. The structural acoustic approach to target detection and identification offers significant advantages over more conventional acoustic approaches which rely only on the formation of high resolution images. Munitions submerged in sea or fresh water for any length of time may become heavily rusted or encrusted with sea growth. At present there is very little hard empirical data on the effects of corrosion and biofouling in marine environments on EMI and acoustic signature variability. Such data are needed for the success of UXO detection and classification in the underwater environment.

This research systematically examines the effects of two primary types of corrosion and biofouling that are commonly found in the underwater environment. A combination of laboratory tank tests and controlled exposure in real-world underwater environments were used.

Reliable methods for accelerated production of calcareous biofouling and magnetite corrosion layers in a controlled laboratory environment were developed for our standard munitions surrogate. Several batches of the surrogate underwent environmental exposure for increasing biofouling layer development over time. Two inert munitions, a 155mm projectile and a 5-in rocket warhead, underwent environmental exposure to develop biofouling layers as well. Further, the inert munitions, after cleaning, were exposed to an accelerated production of magnetite corrosion.

The biofouled and magnetite-corroded surrogates showed no measurable difference in the EMI response when measured in artificial sea water and when measured in air. No measurable difference was seen between bare surrogates and those with the corrosion layers applied. A small difference was observed for laboratory-generated calcareous deposits for one EMI response axis only. This result was potentially corroborated by contact, electrochemical measurements made on samples continuously exposed long term to seawater.

Low frequency (structural acoustic domain) acoustic scattering measurements made on the two biofouled shells together with subsequent analysis demonstrated the following. Overall the biofouling has affected the scattering levels a small amount but not the overall acoustic color frequency-angle spectra. The robustness of the acoustic color spectra bodes well for the performance of RVM classification algorithms. We conclude without specifically demonstrating it that there would be little impact on acoustic detection ranges, classification performance, or maximum burial depth caused by a thin corrosion layer. Regarding the measurements made over the high frequency (conventional imaging regime), the specular echo is affected only in a minor way by biofouling. Finally, the thin corrosion layer has no noticeable effect on acoustic response over almost the entire high-frequency band.

Contents

Abstract i
Contents ii
Figures iii
Acronyms v
Objective 1
Technical Approach 2
Background 2
Approach 4
Laboratory-Accelerated Corrosion 4
Environmental Exposure 6
EMI Response Signature Measurements 8
Structural Acoustics Response Signature Measurements 10
Results and Discussion 11
Accelerated Corrosion and Simulated Biofouling 11
Calcareous Deposits 11
Magnetite Layer Formation 12
EMI Measurements 13
Electrochemical Characterization of Steel 16
Early-Time EMI Response 17
Physical Acoustics Measurements 17
Objective 19
Technical Approach 20
Results 20
Benefits 21
Conclusions 22
Literature Cited 23

Figures

Figure 1 – Examples of fouled and corroded munitions recovered from underwater. 2
Figure 2 – EMI signatures of 10 cm diameter steel sphere with 0, 1mm, …, 5 mm thick corrosion layer having properties (a) $\sigma = 2.5x10^4$ S/m, $\kappa = 20$, and (b) $\sigma = 7.5x10^5$ S/m, $\kappa = 4$. 3
Figure 3 – (left) Small ISO, (right) solid steel surrogate. 4
Figure 4 – Schematic exposure procedure for controlled growth of magnetite corrosion layer..... 5
Figure 5 – (left) Experimental setup for growth of calcareous deposits, (right) Calcareous deposit formation chemistry 5
Figure 6 – (left) a rack of UXO surrogates prior to exposure, (right) a rack of UXO surrogates after 8 weeks of exposure. 6
Figure 7 – Photographs of the 155mm Howitzer shell and 5-inch rocket. 6
Figure 8 – (left) 155mm Howitzer shell, (center) 5-inch rocket, and (right) Test setup on dock... 7
Figure 9 – Time series of biofouling of the inert 155mm projectile at 0, 2, 4, 10, and 16 weeks. . 7
Figure 10 – Time series of biofouling of the inert 5-in rocket at 0, 2, 4, 10, and 16 weeks. 7
Figure 11 – (left) MR-2409 DAQ and electronics, (right) MR-2409 sensor assemblies in the water with an ellipsoidal test object in position. 8
Figure 12. Basic test setup. Sensors and targets are attached to a fiberglass grate which can be raised above and lowered into the 6000 gallon (10-ft diameter by 11-ft deep) plastic tank..... 9
Figure 13 – (Upper Left) Magnetite sample in air, (Upper Right) Calcareous sample in water, (Lower Left) Biofouled sample in air, (Lower Right) Biofouled sample in water 10
Figure 14 – Target strength vs frequency (semi-log) and aspect angle - acoustic color - for a simulant-filled 5-inch rocket. Measured (left); Rigid body response (right). 11
Figure 15 – Progression of Calcareous Deposit Formation, increased exposure time from left to right 12
Figure 16 – Electrochemical impedance spectra of steel surrogate before calcareous deposit formation (blue) and after an hour of calcareous deposition formation (red). Impedance increases as the deposit forms in the 1-10 Hz range. 12
Figure 17 – XRD spectrum of surrogate (blue) and magnetite reference (red). Shaded regions shows where small surface peaks of the surrogate line up with the magnetite reference spectrum. 13
Figure 18 – 1-in steel surrogate with various corrosion (left), and biofouling (right) examples.. 13
Figure 19 – Example results for biofouled samples, both in water and in air. 14
Figure 20 – Second round of biofouled munitions surrogates 15
Figure 21 – EMI Response Results for Calcareous Coatings on Surrogates in Water versus in Air 15
Figure 22 – Calcareous Films Grown on 4-inch Diameter Spheres (left) Steel and Aluminum (left to right), and (right) Aluminum with Calcareous film, bare Aluminum, and bare Steel (left to right). 16
Figure 23 – EIS results for steel surrogates with (left) a magnetite coating, and (right) a calcareous layer, 12-month magnetite results for reference. 16

Figure 24 – Early-time EMI measurements of a sample with (left) a magnetite coating, and (right) a calcareous deposit. An original TEMTADS coil with a z-axis receiver is shown in the center. 17
Figure 25 – NRL Laboratory for Structural Acoustics. A one-million gallon pool facility with adiabatic walls and acoustic coatings, vibration isolation system, and complex acoustic scanners, sources, and processing algorithms. 18
Figure 26 – Experimental Measurement Geometry. The target is placed in the plane-wave, near-field region of a cylindrical source array having a nearly co-located broadband short vertical receiver array or in the farfield of a piston source. The target (which is ~ 2.8 m from the receiver) is rotated over a full 360 degrees in increments of 1 degree. 19

Acronyms

cDAQ	Compact Data Acquisition System
DENIX	Department of Defense Environment, Safety and Occupational Health Network and Information Exchange
EIS	Electrochemical Impedance Spectroscopy
EMI	Electromagnetic Induction
ESTCP	Environmental Security Technology Certification Program
LDV	Laser Doppler Vibrometry
LSA	Laboratory for Structural Acoustics
NAH	Nearfield Acoustic Holography
PVC	Polyvinyl chloride
Rx	Receive
SERDP	Strategic Environmental Research and Development Program
SNR	Signal to Noise Ratio
TEM	Transient Electromagnetic
TEMTADS	Transient Electromagnetic Towed Array Detection System
Tx	Transmit
UXO	Unexploded Ordnance
XRD	X-ray Diffraction

Objective

The objective of this project is to determine the effects of corrosion and biofouling on the electromagnetic induction (EMI) and physical acoustic response signatures of military munitions located at underwater munitions response sites. On land, advanced EMI sensor arrays have been demonstrated to reliably detect and classify buried UXO at real munitions response sites under operational conditions. A similar capability does not yet exist for the marine environment, which is receiving increased attention for remediation efforts. The structural acoustic approach to target detection and identification offers significant advantages over more conventional acoustic approaches which rely only on the formation of high resolution images. Munitions submerged in sea or fresh water for any length of time may become heavily rusted or encrusted with sea growth. At present there is very little hard empirical data on the effects of corrosion and biofouling in marine environments on EMI and acoustic signature variability. Such data are needed for the success of UXO detection and classification in the underwater environment. This research systematically examines the effects of two primary types of corrosion and biofouling that are commonly found in the underwater environment. A combination of laboratory tank tests and controlled exposure in real-world underwater environments were used. The results of this project will provide valuable information to the UXO/Clutter classification process for projects in the marine environment in terms of the expected responses of UXO located in the marine environment. The laboratory and data analysis techniques developed and refined for this project will provide a guide for how to adapt existing land-based data to the marine environment as well.

Technical Approach

Background

On land, the Environmental Security Technology Certification Program (ESTCP) Classification Pilot Program Live Site Demonstrations have demonstrated that the advanced EMI sensor arrays emerging from Strategic Environmental Research and Development Program (SERDP)- and ESTCP-sponsored research can be used to reliably detect and classify buried UXO at real-world munitions response sites under operational conditions. A similar capability does not yet exist for the marine environment. Serious research, development, and testing of EMI systems for underwater UXO detection and classification have only recently begun. One promising avenue for underwater UXO classification emerging from SERDP funding is the use of structural acoustics to develop a diverse set of spatial and spectral structural acoustic "fingerprints" and provide low-frequency sediment penetration permitting buried target prosecution.

Munitions submerged in sea or fresh water for any length of time may become heavily rusted or encrusted with sea growth. An example is shown in Figure 1, taken from the DENIX (Department of Defense Environment, Safety and Occupational Health Network and Information Exchange) pamphlet "Maritime Industry Safety Guide." [1] The effects of such fouling and corrosion on the response signatures used to classify targets as munitions or clutter have not been thoroughly addressed.

Figure 1 – Examples of fouled and corroded munitions recovered from underwater.

EMI detection and classification of UXO has a rich and now-successful history for land-based applications. Less is known in the marine environment. In the course of SERDP project MR-1321, Geophex found, using the GEM-3 frequency-domain sensor, that an insulating layer around a metal target could drastically change the current-channeling (galvanic) response that is observed in conducting media [2]. This has been corroborated for time-domain sensors in

SERDP project MR-2409 [3]. The eddy current response may also be affected. In SERDP Project MR-1632, Shubitidze considered the effect of an insulating skin acquired through corrosion and concluded that the effects on the eddy current response would not be very noticeable for thin shells and at the usual EMI frequencies [4]. However, this model does not capture all of the relevant phenomenology. As noted above, the current channeling response will be affected by an insulating layer, and a thick series of calcareous layers from cathodic corrosion reactions and hard biofouling have been shown to reduce current channeling [5,6]. Furthermore, some corrosion products, such as Fe_3O_4 (magnetite) and gamma phase Fe_2O_3 (maghemite), are electrically conducting and magnetic, which would likely produce a more significant effect on the eddy current response than is seen in Shubitidze's calculations. Preliminary calculations have predicted that the presence of these corrosion products can alter the eddy current response (Figure 2). We have calculated the response of a 10 cm diameter steel sphere with an outer corrosion layer ranging in thickness from 0 to 5 mm in steps of 1 mm using standard theory for the transient EMI (TEM) response of a layered sphere [7]. Zou *et al.* [8] report magnetite layers 1-2mm thick on steel test coupons after 48 week of exposure to seawater. Additionally, they observed that the magnetite layer increased in thickness over time. Given these observations it is reasonable to assume that a magnetite layer reaching a thickness of 5mm could be achieved with exposure periods longer than 48 weeks. For the left-hand plot (a) we modeled the corrosion layer using nominal conductivity (σ) and relative permeability (κ) values for magnetite of $2.5\text{x}10^4$ S/m and 20, respectively [9,10]. For the right-hand plot (b) we used $\sigma = 7.5\text{x}10^5$ S/m and $\kappa = 4$, which are values reported by Gotoh *et al.* [11] for a rust layer on carbon steel. Conductivity and permeability values of $4.68\text{x}10^6$ S/m and 60, respectively were used for the inner steel ball in both cases.

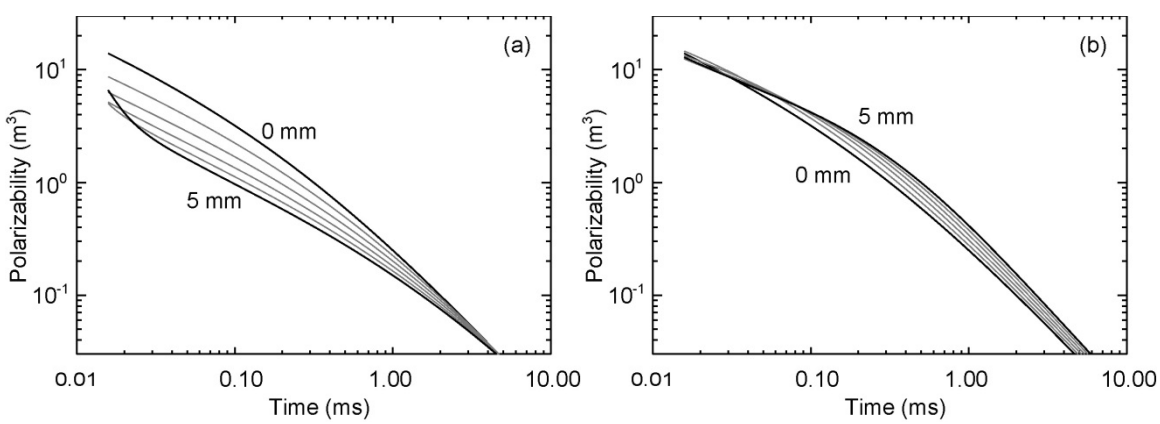

Figure 2 – EMI signatures of 10 cm diameter steel sphere with 0, 1mm, …, 5 mm thick corrosion layer having properties (a) $\sigma = 2.5\text{x}10^4$ S/m, $\kappa = 20$, and (b) $\sigma = 7.5\text{x}10^5$ S/m, $\kappa = 4$.

A number of SERDP Projects (MR-1513, MR-1665, MR-2103, MR-2230, for example) have been exploring structural acoustics (SA) based sonar methodology [12] for detection and classification of underwater unexploded ordnance (UXO). The structural acoustic approach to target detection and identification offers significant advantages over these more conventional

acoustic approaches which rely only on the formation of high resolution images. These advantages include a diverse set of spatial and spectral structural acoustic "fingerprints" leading to high probability of detection, low false alarm rates and low frequency sediment penetration permitting buried target prosecution. These and related efforts have generated a growing library of what are called "acoustic color" data bases (acoustic scattering versus frequency and aspect) for a variety of UXO targets. It is from these acoustic color maps that classification features are derived. For the most part, these data bases do not include targets that are corroded or biofouled so that there is no understanding regarding how structural acoustic features might be altered by these effects.

Approach

Our approach was comprised of four elements: (1) accelerated corrosion and simulated biofouling of munitions surrogates in a controlled laboratory environment, (2) simultaneous environmental exposures of munitions items and surrogates, (3) Measurement of a) EMI, and b) structural acoustic response signatures of corroded and biofouled munitions items and surrogates, and (4) physical modeling to develop a framework for predicting the impact of corrosion and biofouling on UXO / Clutter classification methodologies for use in munitions response activities. EMI response signature measurements were made of the samples at our underwater EMI test facility at Blossom Point, MD, both in air and in artificial sea water. Acoustic measurements were made in a tank facility at NRL-DC.

For the munitions surrogate, the chosen item is readily available in large quantities. Like the small Industry Standard Object (ISO) [13], shown in Figure 3 (left), currently used in land-based munitions response (MR) projects, we used a solid bar of carbon steel cut to 4-in long x 1-in OD, approximately the length of a 37mm. Figure 3 (right) shows a surrogate cleaned and ready for simulated fouling.

Figure 3 – (left) Small ISO, (right) solid steel surrogate.

Laboratory-Accelerated Corrosion

NRL's Center for Corrosion Science and Engineering (Code 6130) has a well-established record in characterizing and reproducing corrosion and biofouling effects in the field and in laboratory settings [14,15]. Using a series of laboratory-accelerated corrosion techniques developed by

NRL Code 6130, we have investigated two main contributions to marine corrosion and biofouling individually. Magnetite (Fe_3O_4) is a common corrosion product in the marine environment. A ferrimagnetic material, the presence of an outer magnetite layer may alter the measured EMI response. Laboratory-accelerated corrosion was used to produce specimens with a magnetite corrosion product using polarizations of carbon steel in hot alkaline solutions. Exposure conditions were tuned to specifically produce a thin film of magnetite, and not hematite (Fe_2O_3). The process is outlined schematically in Figure 4. X-ray diffraction (XRD) analysis was used to verify corrosion products.

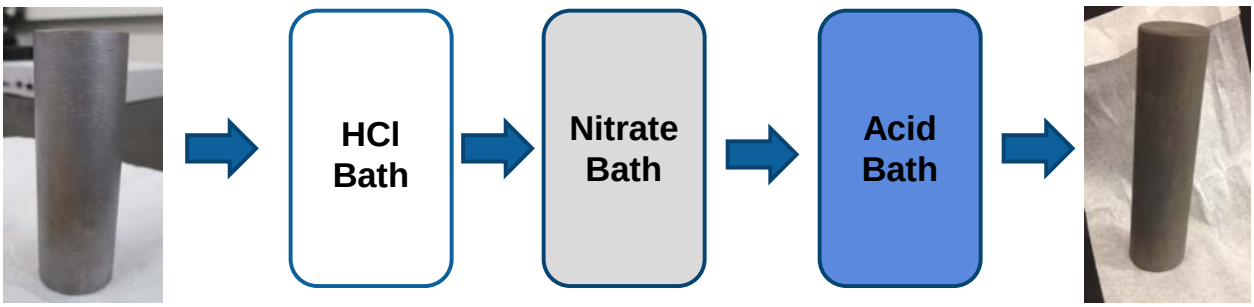

Figure 4 – Schematic exposure procedure for controlled growth of magnetite corrosion layer

Calcareous deposition and growth on laboratory specimens was achieved through cathodic polarizations in artificial sea water. These conditions simulate the effects of calcareous shell deposition and growth at the solid/liquid interface, typically observed in barnacle (cyprid) and tubeworm (spirorbid) settlement and growth. The samples are placed in a bath composed of NaCl / Ca_2SO_4 (Calium Sulfate) / $MgSO_4$ bath. The samples are then polarized to form a localized basic environment to cause products to form (precipitation), as outlined in Figure 5.

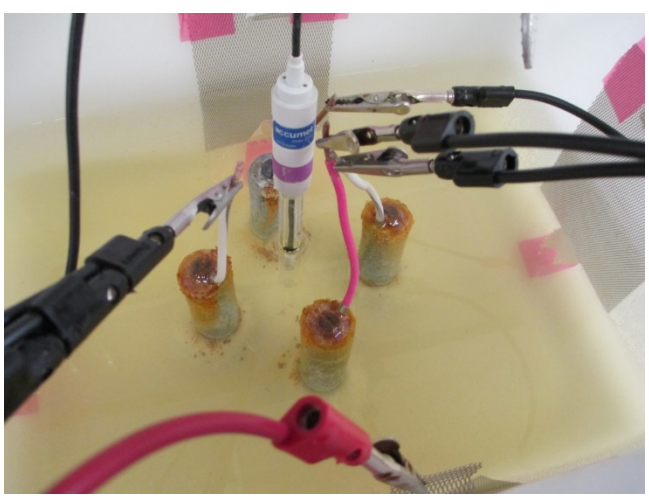

$$\mathbf{2\,H_2O + 2e^- \rightarrow H_2 + 2OH^-}$$

$$CO_2 + OH^- \rightarrow HCO_3^-$$

$$OH^- + HCO_3^- \rightarrow H_2O + CO_3^{2-}$$

$$CO_3^{2-} + Ca^{2+} \rightarrow CaCO_{3(s)}$$

Figure 5 – (left) Experimental setup for growth of calcareous deposits, (right) Calcareous deposit formation chemistry

Environmental Exposure

In parallel to the accelerated laboratory sample preparation, we conducted surrogate environmental exposures at a real-world site for comparison and eventual model validation. Code 6130 regularly utilizes a facility near Miami, FL for hard fouling testing. The site contains an aggressive fouling community with a high percentage of hard fouling species. Figure 6 shows examples of the surrogates prior to exposure and at an intermediate point in the exposure period.

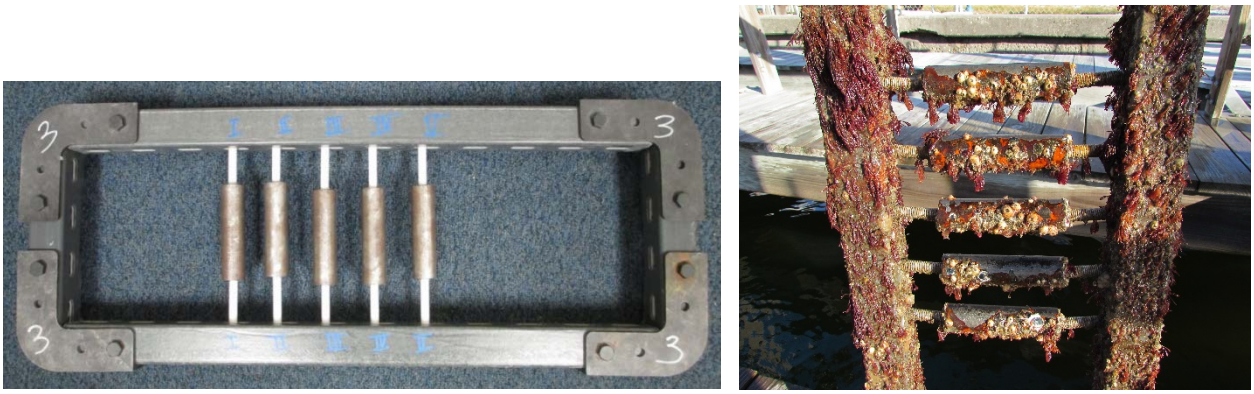

Figure 6 – (left) a rack of UXO surrogates prior to exposure, (right) a rack of UXO surrogates after 8 weeks of exposure.

In addition to studies of the standardized UXO surrogate, two inert UXOs, filled with an epoxy material, were exposed to corrosion and biofouling under real-world conditions. We have these items in our inventory and extensive structural acoustics studies have already been conducted on them. These are the 155mm Howitzer shell and the 5-inch rocket shown in Figure 7.

Figure 7 – Photographs of the 155mm Howitzer shell and 5-inch rocket.

In February 2016, the two items were shipped to Code 6130's site in Florida for environmental exposure. Figure 8 shows the two items prepared for immersion in Florida. Photographic time series of the biofouling exposures are shown in Figure 9 and Figure 10.

Figure 8 – (left) 155mm Howitzer shell, (center) 5-inch rocket, and (right) Test setup on dock

Figure 9 – Time series of biofouling of the inert 155mm projectile at 0, 2, 4, 10, and 16 weeks.

Figure 10 – Time series of biofouling of the inert 5-in rocket at 0, 2, 4, 10, and 16 weeks.

EMI Response Signature Measurements

Advanced EMI response data were collected using the advanced EMI system developed for underwater UXO characterization in SERDP Project MR-2409. The underwater system is configured with a single transmitter coil and two triaxial receiver cubes, shown in Figure 11. The MR-2409 system, much like our previous TEMTADS HandHeld (HH) sensor [16], is not currently configured to simultaneously collect the same rich, bistatic data sets as advanced EMI arrays. As such, they both must use a dense, template-based data collection methodology for collecting classification-grade EMI data. The same approach was used by Geophex in their pioneering data collection in MR-1321.

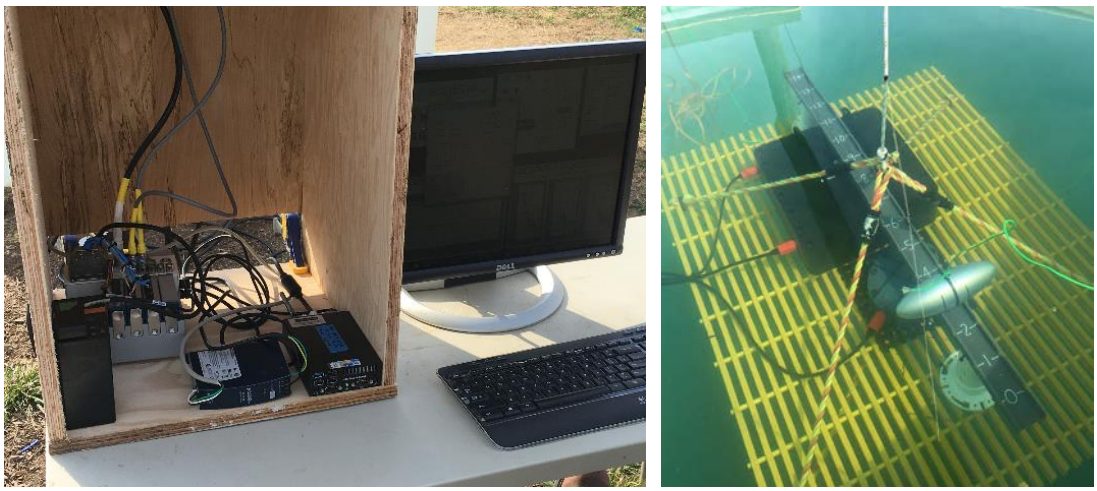

Figure 11 – (left) MR-2409 DAQ and electronics, (right) MR-2409 sensor assemblies in the water with an ellipsoidal test object in position.

Testing was done at the Naval Research Laboratory's EMI Underwater Test Facility at Blossom Point, MD. The basic test setup is shown in Figure 12. A 10-ft diameter by 11-ft deep (3.05 m x 3.35 m), 6000 gallon (22.7 kL) industrial plastic tank was partially buried and filled with a salt water solution. The salinity of the tank water was 35‰. During the course of the testing water temperatures ranged from less than 5° C to 25° C. At various times the electrical conductivity of the water was measured using a Hanna Instruments HI98304 DIST4 electrical conductivity sensor (using samples diluted with distilled water for conductivities greater than 2 S/m). At specific salinities, conductivity as a function of temperature was determined using standard tables and formulae [17]. All of the data in support of this project, MR-2500, were collected at 35‰, with conductivity in the range 3.2-4.5 S/m. The water in the tank was mixed with a removable pump each day before the start of testing to eliminate temperature and salinity stratification.

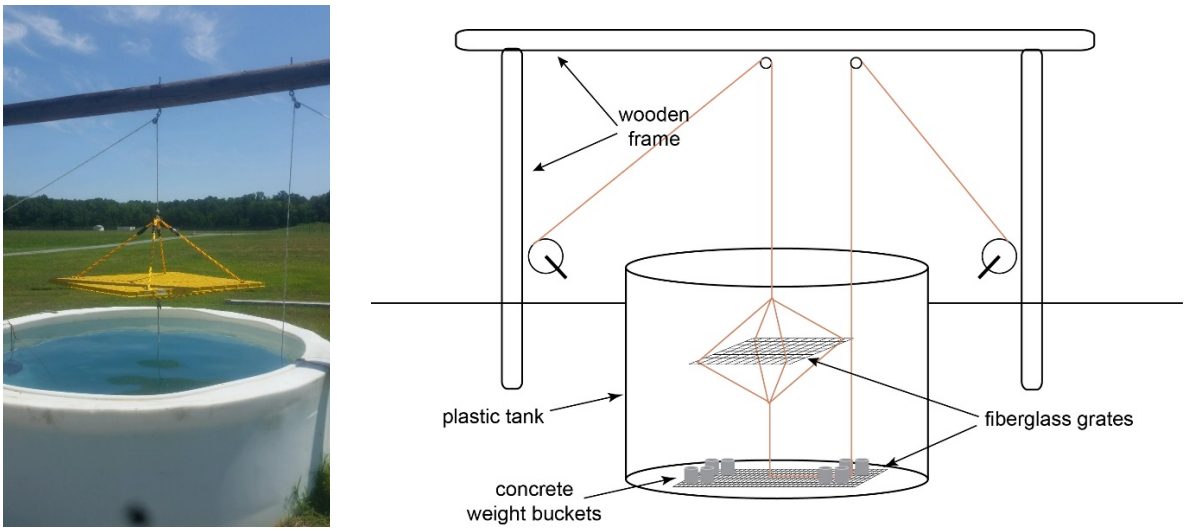

Figure 12. Basic test setup. Sensors and targets are attached to a fiberglass grate which can be raised above and lowered into the 6000 gallon (10-ft diameter by 11-ft deep) plastic tank.

Sensors and targets were attached to a fiberglass grate which could be winched up above the tank or down into the water. The basic test protocol involved repeating measurements with and without a target in the water and then again in air with the rig pulled out beside the tank. This allowed background response contributions to be removed from the target response measurements and allowed for direct in water and in air comparison. In addition to the test setup shown in Figure 11, data on corroded samples were collected with a larger, 1-m x 0.5m transmitter array constructed for MR-2409's efforts and a single, triaxial receiver cube in a prototype water housing was used, as shown in Figure 13.

The coils were driven with a new compact version (cDAQ) of the TEMTADS 2X2 electronics developed by G&G Sciences. The data acquisition electronics were placed on a table roughly five meters from the tank. The acquisition computer was powered from an available 60 Hz AC line. The transmitter and receiver electronics were powered from a battery. The system is capable of generating a variety of bipolar transmit waveforms, as well as being flexible in stacking and time gating the measured transient decays. The standard TEMTADS pulse duration of 25 ms was used. Peak transmit currents were between 5 and 6 A. Raw transients sampled at 250 kHz were recorded for noise studies. For background and target response measurements roughly 200 decays were averaged and 121 logarithmically spaced time gates (5% gate width) were recorded, the last 100 or so of which (corresponding to decay times greater than about 0.1 ms) are typically used for target classification.

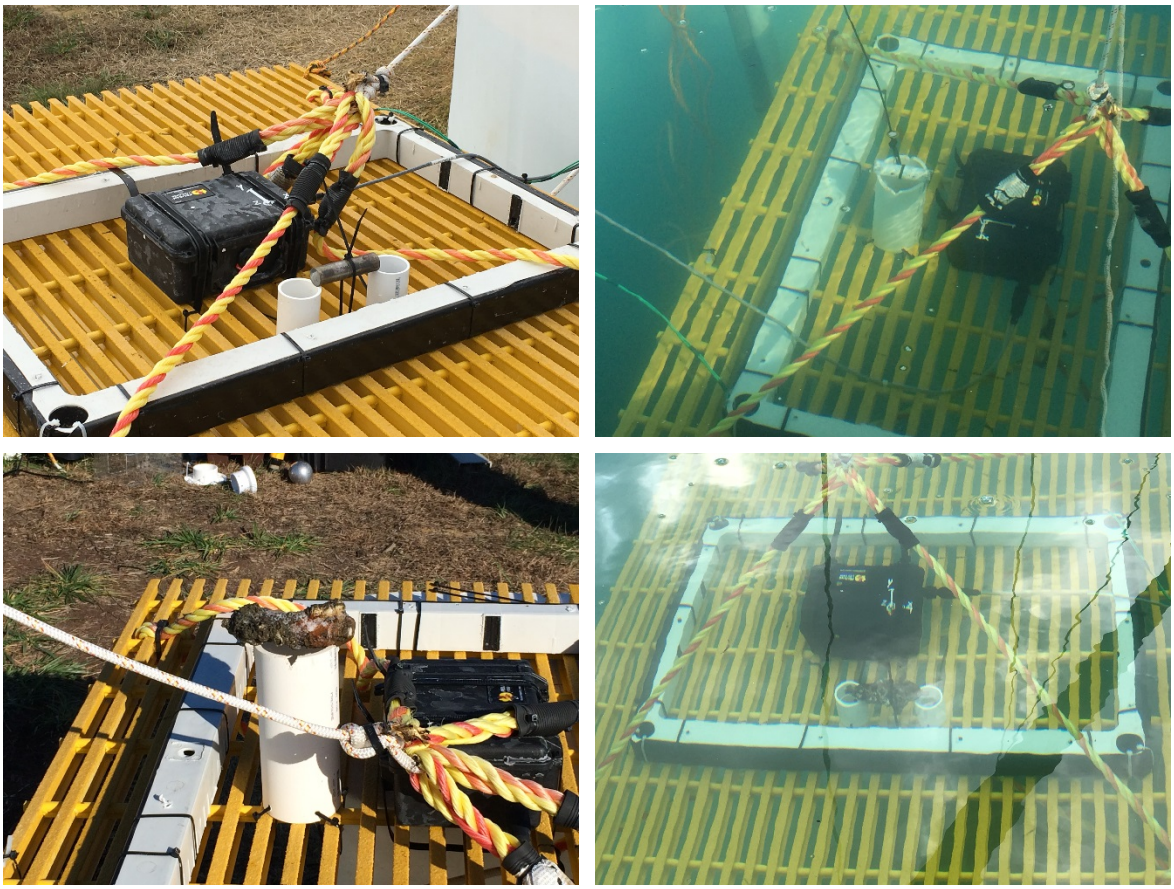

Figure 13 – (Upper Left) Magnetite sample in air, (Upper Right) Calcareous sample in water, (Lower Left) Biofouled sample in air, (Lower Right) Biofouled sample in water

Structural Acoustics Response Signature Measurements

For the structural acoustics measurements, the objective was to determine the effects of corrosion and biofouling on a UXO target's acoustic color map. We show on the left in Figure 14 the acoustic color map measured for a 5-inch rocket filled with an epoxy material. [18] On the right is shown the acoustic color map that would result were the target perfectly rigid, *i.e.* the case in which no acoustic energy penetrates the target. The detailed frequency/angle structure in the measured map on the left provides effective "fingerprinting" features for the classification algorithm. Once the environmental exposure of the UXO were complete, color maps for the corroded targets were measured and the differences between the acoustic color for a pristine target versus that for a corroded target determined. Further, the effect of corrosion on the various structural acoustic mechanisms which lead to these features were examined. As an example, the color map on the right in Figure 14 for a rigid rocket is a good approximation for the specular scattered component in the acoustic echo. The specular component is of interest since it is used to form an acoustic image which provides direct identification information such as size and shape.

These acoustic scattering measurements were carried out in NRL's Laboratory for Structural Acoustics Facility, a state-of-the-art, 1M gallon, controlled and highly instrumented in-ground pool. The measurements were made over the broad frequency band shown in Figure 14, *i.e.* 2 kHz to 140 kHz and over a full 360 degrees in steps of one degree.

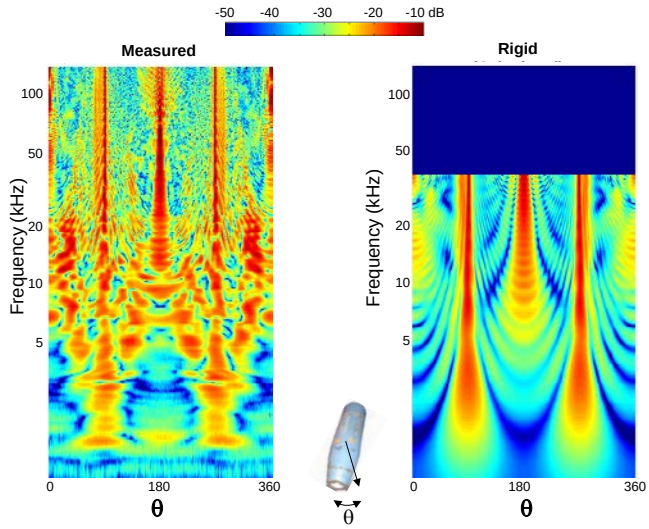

Figure 14 – Target strength vs frequency (semi-log) and aspect angle - acoustic color - for a simulant-filled 5-inch rocket. Measured (left); Rigid body response (right).

Further details on the technical approach for the structural acoustics effort can be found in Reference 19.

Results and Discussion

The organization of this Section will mirror that of the technical approach. Four elements are discussed: (1) accelerated corrosion and simulated biofouling of munitions surrogates in a controlled laboratory environment, (2) simultaneous environmental exposures of munitions items and surrogates, (3) Measurement of a) EMI, and b) acoustic signature response signatures of corroded and biofouled munitions items and surrogates, and (4) physical modeling to develop a framework for predicting the impact of corrosion and biofouling on buried, unexploded ordnance (UXO) / Clutter classification methodologies for use in munitions response activities.

Accelerated Corrosion and Simulated Biofouling

Calcareous Deposits

Without cathodic protection, ions from the ocean will react on metal surfaces and form films of calcium carbonate ($CaCO_3$) and magnesium hydroxide ($Mg(OH)_2$). These layers should be insulating and may affect the measured responses for UXO. Cleaned, bare steel surrogates were placed in a localized basic environment, as described above, and precipitates were allowed to

form. A time series is shown in Figure 15. The formation of the calcareous layer is monitored using electrochemical impedance spectroscopy (EIS), as shown in Figure 16.

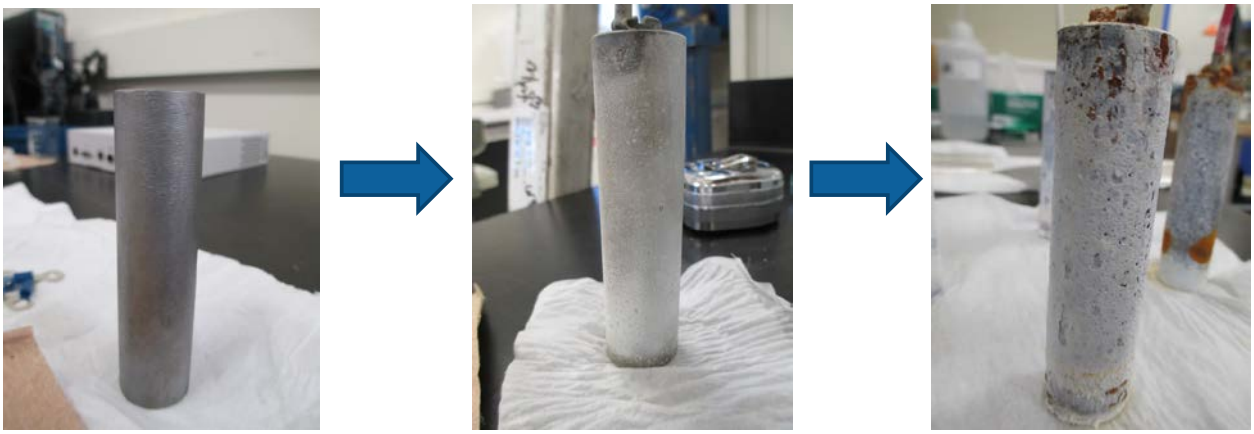

Figure 15 – Progression of Calcareous Deposit Formation, increased exposure time from left to right

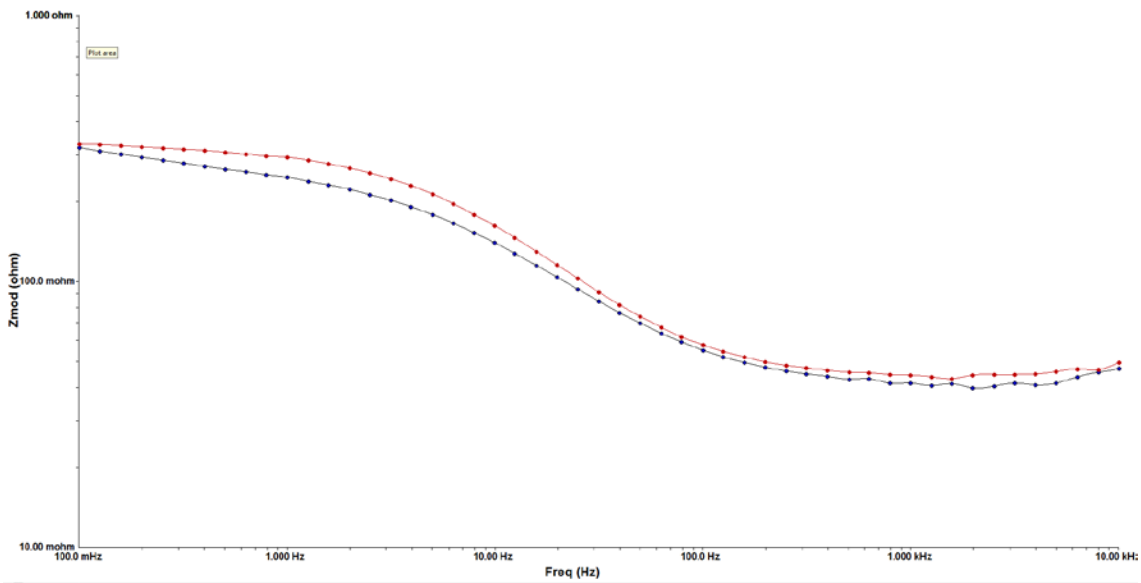

Figure 16 – Electrochemical impedance spectra of steel surrogate before calcareous deposit formation (blue) and after an hour of calcareous deposition formation (red). Impedance increases as the deposit forms in the 1-10 Hz range.

Magnetite Layer Formation

Magnetite (Fe_3O_4) is a common corrosion product in the marine environment. A ferrimagnetic material, the presence of an outer magnetite layer on a specimen may alter the measured EMI response. Cleaned, bare steel surrogates were placed in a series of baths, as described above, and a corrosion layer was allowed to form. Exposure conditions were tuned to specifically produce a thin film of magnetite, and not hematite (Fe_2O_3). The thickness of the corrosion layer produced

was not quantitatively measured, but the technique used typically creates magnetite films approximately 1mm thick. XRD analysis of surrogate showed a large Fe signature attributed to the bulk of the specimen and small peaks of a thin magnetite coating, as shown in Figure 17.

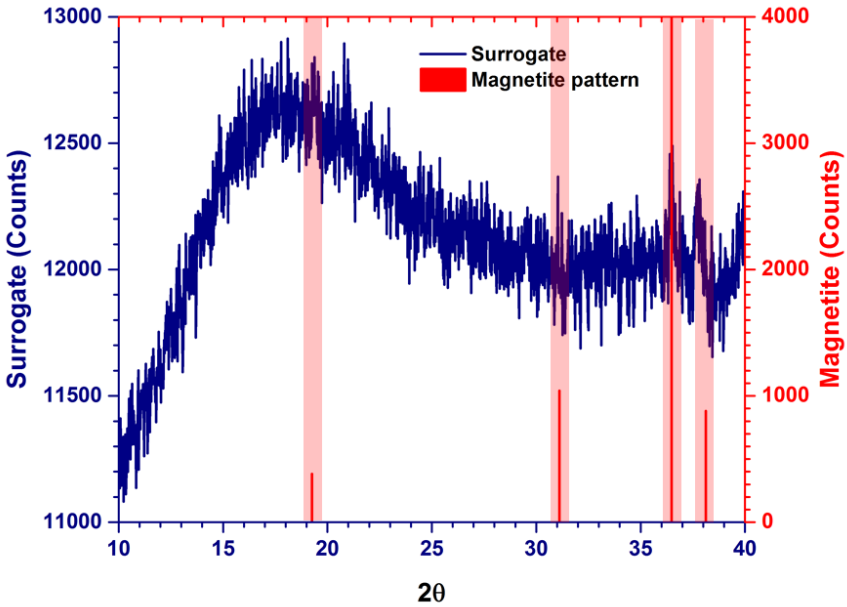

Figure 17 – XRD spectrum of surrogate (blue) and magnetite reference (red). Shaded regions shows where small surface peaks of the surrogate line up with the magnetite reference spectrum.

EMI Measurements

The first set of samples measured with an advanced EMI sensor system were formed on 1-in diameter, 4-in long solid steel bars, as shown in Figure 18. The laboratory-fouled samples are shown on the left. The biofouled samples were exposed for 12 months, and are shown on the right.

Figure 18 – 1-in steel surrogate with various corrosion (left), and biofouling (right) examples

All of these items have a common base object, the 1-in diameter steel rod. This allowed the measurements to be made with the steel rod in a consistent location. Controlling the sample location leads to a well-defined transmitter loop / sample / receiver loop geometry, minimizing the effects of measurement geometry on the collected data. This allows us to focus on any impact from the coatings. Examples of this measurement protocol are shown in Figure 13.

For the first batch of biofouled samples, shown in Figure 18 (right), there was no measurable difference for the samples in water. The baseline in-air measurments showed no measurable difference, as well. Example data are shown in Figure 19 for the vertical (Z) and horizontal (X,Y) receiver loops.

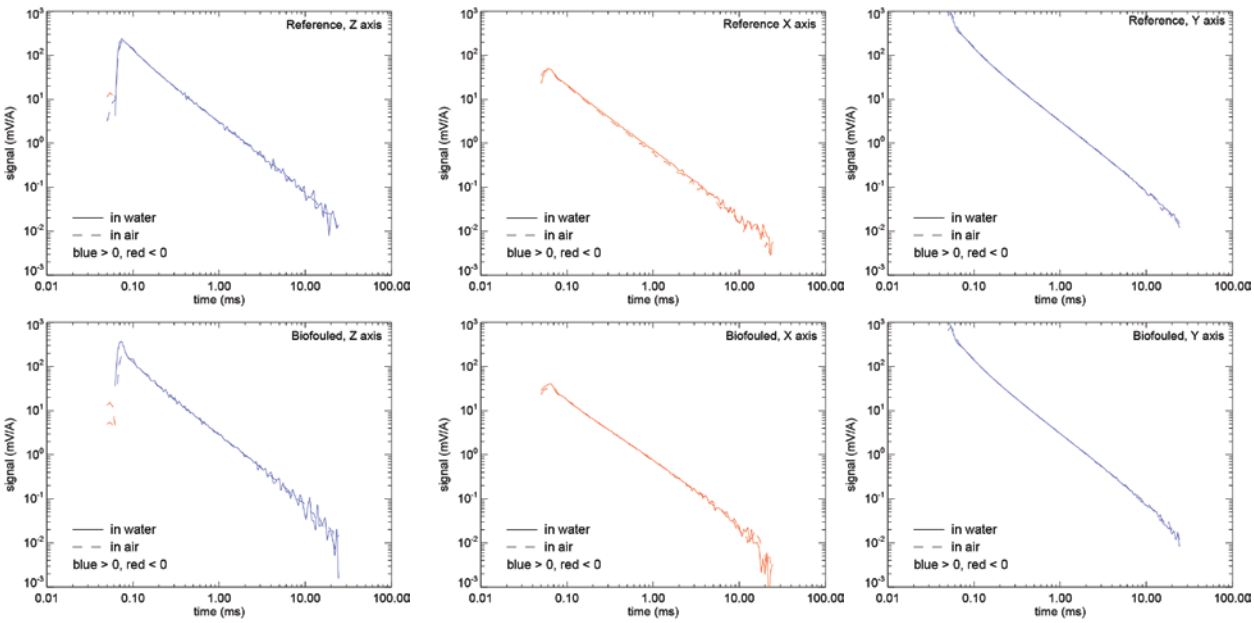

Figure 19 – Example results for biofouled samples, both in water and in air.

A second batch of biofouled samples was removed from the water in April, 2016, roughly 4 months after the first batch. The samples are shown in Figure 20. Once again, no difference between in water and in air EMI measurements was observed.

For the calcareous samples, the white-coated samples as seen in Figure 18 (left), no difference in response was seen for the vertical (Z) or horizontal (Y) receiver loop response, as seen in Figure 21. A small difference is seen in the horizontal (X) receiver loop response when the calcareous deposit is present, which is counterintuitive. The current channeling response, which would be suppressed by calcareous deposits, should be the strongest in the Y- and Z-axis components of the response for the measurement configuration used. Refer to Figure 13, lower right. The initial measurement design for these experiments was susceptible to flexure of the experimental jig and small positioning offsets from object to object. As a result, the difference observed may be experimental.

Figure 20 – Second round of biofouled munitions surrogates

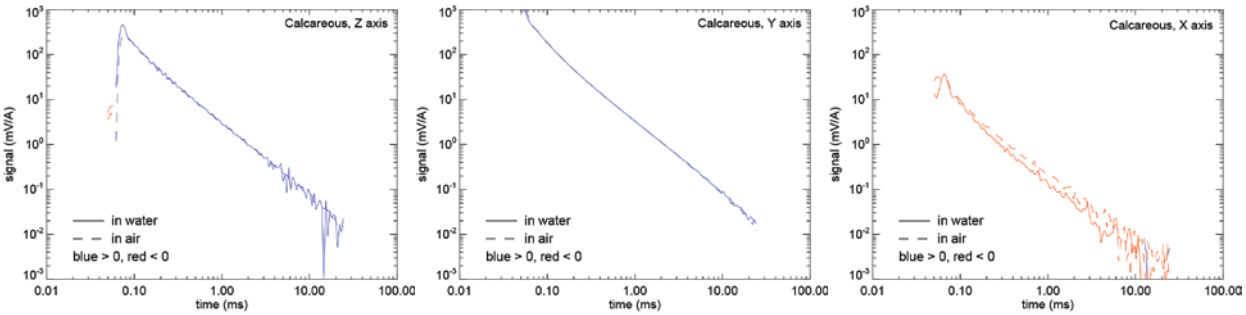

Figure 21 – EMI Response Results for Calcareous Coatings on Surrogates in Water versus in Air

A second set of measurements were undertaken with calcareous deposits to further explore this issue. Two 4-in diameter spheres, one aluminum and one steel, were exposed to the same accelerated calcareous deposit formation protocol as the 1-in diameter steel rods. The samples are shown in Figure 22. The intent was to form an especially thick layer on each sphere and look for differences both between in air and in water and between coated and not. The larger, symmetric object may led to a more pronounced effect as well. In the case of the aluminum sphere, a uniform film was achieved, but it was much thinner than had been achieved for the rods. For the steel sphere, physical constrains of holding the sphere in the bath led to a non-uniform coating that was again not particularly thick. No differences were observed in the EMI results. We attempted to prepare a new set of samples with better coverage, but were ultimately unsuccessful, perhaps hitting the limit of the facilities / sample preparation technique available to this project.

Figure 22 – Calcareous Films Grown on 4-inch Diameter Spheres (left) Steel and Aluminum (left to right), and (right) Aluminum with Calcareous film, bare Aluminum, and bare Steel (left to right).

Electrochemical Characterization of Steel

In parallel with the laboratory and environmental exposure samples, steel samples were continuously exposed to flow-through sea water at NRL's Key West, FL facility. Samples with magnetite and calcareous coatings were exposed. The sample interface was periodically characterized by EIS. Over the course of a year, the corrosion film changed the EIS response of the sample interface. Calcareous deposits show large changes in interface response, as compared to the magnetite films, as seen in Figure 23. This potentially corroborates the EMI response results shown in Figure 21.

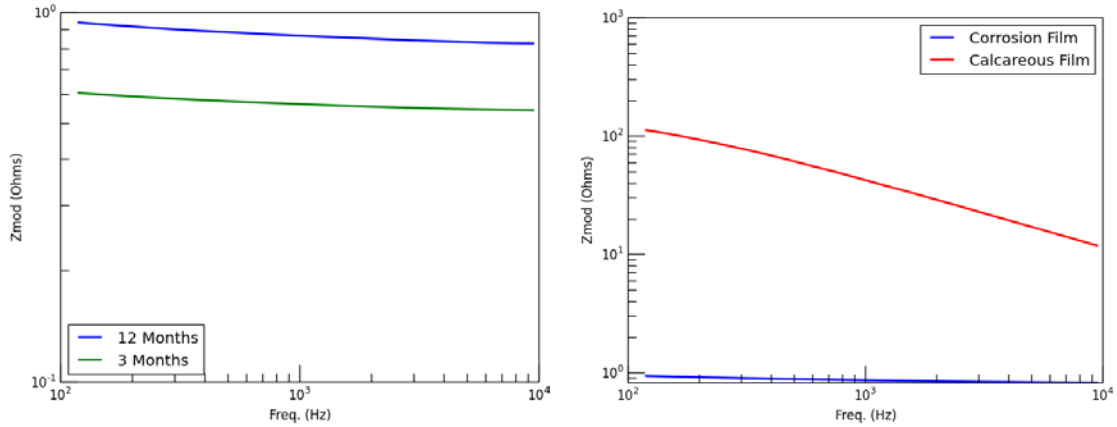

Figure 23 – EIS results for steel surrogates with (left) a magnetite coating, and (right) a calcareous layer, 12-month magnetite results for reference.

Early-Time EMI Response

The EMI results shown so far were all collected using 8-cm triaxial receiver cubes. These are the same receiver cubes using the G&G Sciences MPV series, and are similar in response to the 10-cm receiver cubes used in the Geometrics MetalMapper and MetalMapper 2x2. While the richness of the triaxial response is beneficial to advanced classification data collection, the receiver cubes do not offer the fastest response time available. The original TEMTADS 25-cm, z-axis receiver coil, shown in Figure 24 (center), has a faster response time, allowing for robust data collection as early as 42 μs after the transmitter turn off. By comparison, data from the 8-cm receiver cube is only reliable starting at 89 μs. An original TEMADS sensor was swapped for the TEMTADS/3D coil in the main housing and additional measurements made. It was possible that there might be a difference in the air / water responses only at early time. As can be seen in Figure 24, there is no measureable difference for magnetite (left) and a calcareous coating (right), even at early time.

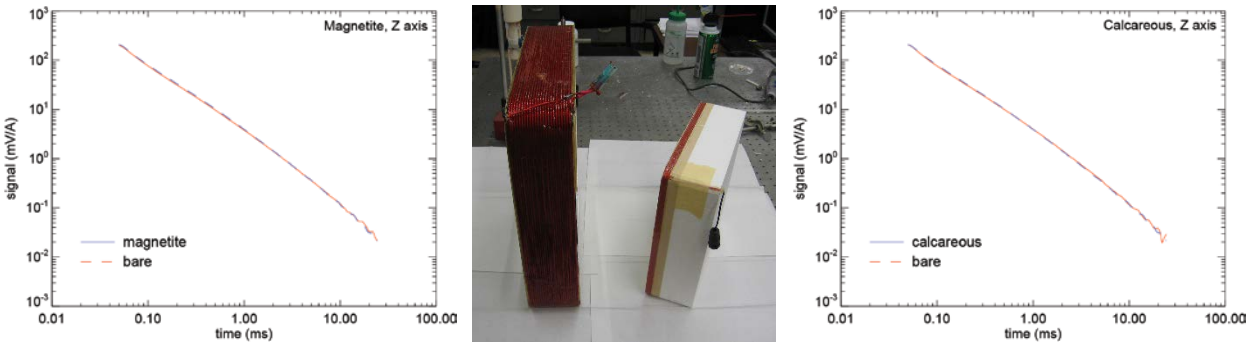

Figure 24 – Early-time EMI measurements of a sample with (left) a magnetite coating, and (right) a calcareous deposit. An original TEMTADS coil with a z-axis receiver is shown in the center.

Physical Acoustics Measurements

The acoustic scattering measurements were carried out at the Laboratory for Structural Acoustics (LSA) at NRL (see Figure 25) which is a state-of-the-art underwater acoustic research laboratory unique in the world. The LSA infrastructure includes a large cylindrical one million gallon (55-ft diameter x 50-ft deep) de-ionized water tank located in Building 5 at NRL. This tank is vibration isolated, temperature controlled, and heavily instrumented with in-water precision robots for nearfield acoustic holography (NAH), laser Doppler vibrometry (LDV), and compact range measurements.

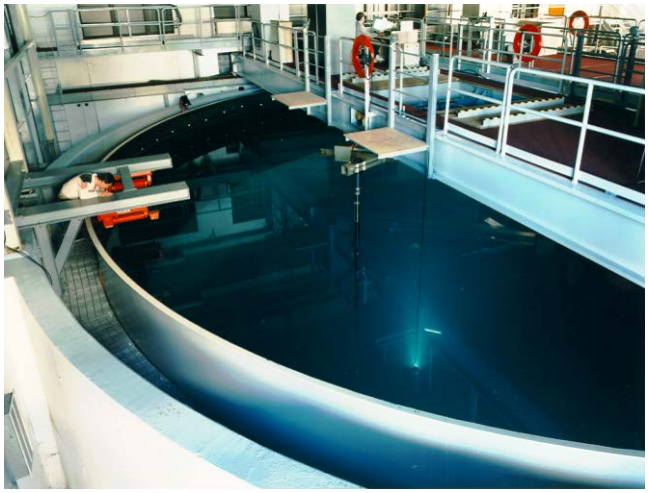

Figure 25 – NRL Laboratory for Structural Acoustics. A one-million gallon pool facility with adiabatic walls and acoustic coatings, vibration isolation system, and complex acoustic scanners, sources, and processing algorithms.

The measurements reported here were conducted with the facility in its compact scattering range mode as shown in Figure 26. Each UXO target was suspended at mid-depth in the tank together with the source and receiver. Two sources were used for these experiments. The first source is a 3 meter long nearfield line array mounted horizontally. The line array generates a broadband pulse approximately 1 ms in duration and covers the band from 1 – 25 kHz. The spatial uniformity of the line array is such that it emulates a farfield plane wave ensonification. The receiver used in these experiments was a vertical line array that is also suspended at the mid-depth of the tank. A second piston-like source is used to collect data in the band from 8kHz – 160 kHz. The measurement system is designed for collection of both monostatic and bistatic scattering data. However, for the measurements reported here, only the monostatic configuration was used, *i.e.* the source and receiver fall along the same bisector to the target center. The scattered echo response was measured 2.7 meters from the target in 1 degree increments over 360 degrees. The data was processed to recover full complex scattering cross-sections expressible as target strength referenced to 1 meter. In this method, the time domain scattered data from the target at a given aspect angle is cleaned to remove unwanted reflections not associated with a target return, is Fourier transformed, and then normalized by a reference measurement.

Measurement Geometry

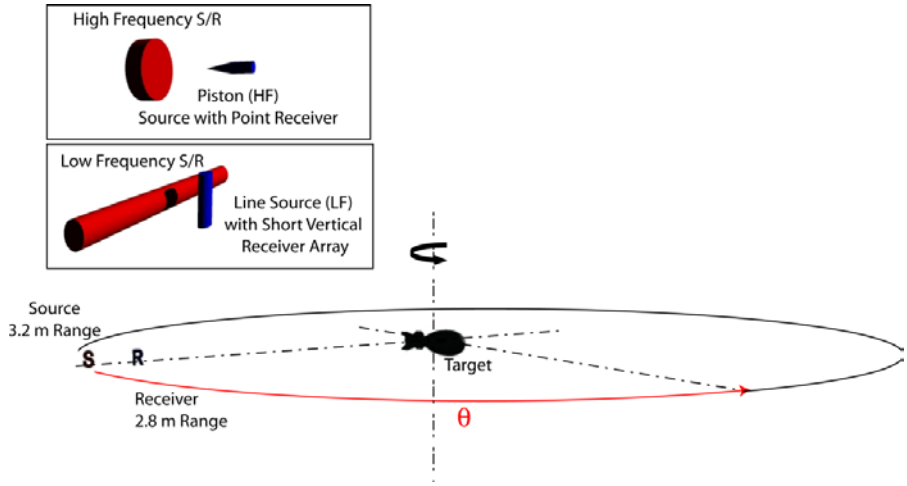

Figure 26 – Experimental Measurement Geometry. The target is placed in the plane-wave, near-field region of a cylindrical source array having a nearly co-located broadband short vertical receiver array or in the farfield of a piston source. The target (which is ~ 2.8 m from the receiver) is rotated over a full 360 degrees in increments of 1 degree.

Further details on the results and discussion for the structural acoustics effort can be found in Reference 19. The Executive Summary of the reference is reproduced here.

Objective

Many active and former military installations have ordnance ranges/training areas with adjacent water environments containing unexploded ordnance (UXO) due to wartime activities, dumping, and accidents. SERDP goals require the development of technologies able to detect and classify UXO, and a number of SERDP projects have been developing structural acoustic (SA) feature-based underwater sonars that can detect and localize buried (and proud) targets separating the detections into UXO vs non-UXO. These and related efforts have generated a growing library of what are called "acoustic color" data bases (acoustic scattering versus frequency and aspect) for a variety of UXO targets. It is from these acoustic color maps that classification features are derived. For the most part, these data bases do not include targets that are corroded or biofouled so that there is little understanding regarding how structural acoustic features might be altered by these effects. Further, the SA sonar methodology includes 3D acoustic imagery where large synthetic apertures created by the sonar's motion allow modest spatial resolution even at the low SA frequencies so that the impact on imagery of biofouling and corrosion is also of interest. Our objective here is to generate a carefully controlled data base determining the effects of corrosion and biofouling on a UXO target's echo characteristics i.e. on "acoustic color" from which both the classification features and images are generated.

Technical Approach

The detailed frequency/angle structure in the measured acoustic color map provides effective "fingerprinting" features for the classification algorithm. Here we measure these color maps for two UXO – a 5" rocket and a 155mm shell both filled with an epoxy resin – and then repeat the measurements after the targets have experienced biofouling and then corrosion. Further, we attempt to determine how the various structural acoustic mechanisms which lead to these features are affected by the biofouling or corrosion. For example, the color map for a rigid rocket is a good approximation for the specular scattered component. The specular component is of interest since it is used to form an acoustic image providing direct classification information such as size and shape. We will attempt to determine how the various mechanisms including circumferential and axial elastic or creeping waves travelling in the shell casing are affected. Finally, we assess the effect of the biofouling and corrosion on the performance of our typical RVM classification algorithm. The acoustic scattering measurements are carried out in NRL's state-of-the-art Laboratory for Structural Acoustics Facility. The measurements are made over the broad frequency band from 2kHz to 140kHz and over a full 360 degrees in steps of one half or one degree. The band is covered by using two facility configurations, one the high frequency arrangement which utilizes a relatively small source and receiver and the other the low frequency system which deploys a large near-field source array to project a plane wave on the nearby target. After baseline scattering measurements are carried out on the "clean" targets, the UXO are exposed for 16 weeks underwater at an at-sea fouling location in Englewood, FL which contains an aggressive fouling community with a high percentage of hard fouling species so that significant biofouling occurred during this relatively short time. After completing acoustic measurements on the biofouled UXO, the shells are cleaned and readied for accelerated corrosion in order to produce magnetite/Hermatite corrosion layers. To accomplish this, the munitions are anodically polarized in a bath of 0.05M NaCl for a week long period such that the corrosion rate is accelerated, simulating ~3 months of seawater exposure. After the corrosion process is completed, the acoustic measurements are repeated once more.

Results

The baseline measurements were analyzed in terms of basic echo mechanisms which included specular scattering from shell ends and cylindrical surfaces, circumferential Rayleigh wave and compressional wave ring resonances, axial compressional and creeping wave interference with specular scattering, elastic wave generation in filler due to phase matching, etc. Low frequency (structural acoustic domain) acoustic scattering measurements made on the two biofouled shells together with subsequent analysis demonstrated the following. Overall the biofouling has affected the scattering levels a small amount but not the overall acoustic color frequency-angle spectra. The level changes, amounting to on average less than 2dB for the 5 inch shell and about 5dB for the 155mm shell, would result in a corresponding drop in signal-to-noise and in turn the related detection ranges. However, the robustness of the acoustic color spectra bodes well for the performance of our RVM classification algorithms. In this regard, both the acoustic color features

and certain pressure magnitude features maintain good UXO classification performance against the set of six non-UXO targets. In particular, pressure magnitude features were shown to separate 4 of 6 false targets from biofouled UXO whereas acoustic color features separated all 6 of 6 false targets from biofouled UXO. Further, we found that biofouling tends to attenuate some axial creeping (~ 1.2 - 1.7 kHz) and circumferential elastic waves (~ 6kHz – 12 kHz) reducing fine structure. This is especially true for 155mm shell. Reduced levels of fine structure are expected to lead to sharper low frequency images since these mechanisms lead to echo time elongation which corrupts the time-delay beamforming processing used in imaging. Regarding the small amount of corrosion achieved in our laboratory attempts to accelerate the corrosion process, except for the apparently anomalous change for the echo from the front and back of both shells at the lowest frequencies and the significant effect on the circumferential Rayleigh wave for the five inch shell, there is as expected no change of any consequence caused by this thin corrosion layer at the low structural acoustic frequencies. We conclude without specifically demonstrating it that there would be little impact on acoustic detection ranges, classification performance, or maximum burial depth caused by this thin corrosion layer. Regarding the measurements made over the high frequency (conventional imaging regime), the specular echo is affected only in a minor way by biofouling, and much of the fine structure due to creeping or elastic axial/circumferential waves is washed out (less true for 155mm shell). Finally, the thin corrosion layer has no noticeable effect on acoustic response over almost the entire band.

Benefits

A number of SERDP Projects have been exploring structural acoustics (SA) based sonar for detection/classification of underwater UXO which offer significant advantages over the more conventional acoustic imaging approaches including a diverse set of spatial and spectral structural acoustic “fingerprints” leading to high probability of detection, low false alarm rates and low frequency sediment penetration permitting buried target prosecution. Further, the SA approach allows the formation through SAS processing of complementary three dimensional images of the sediment volume and of any targets buried therein having sufficient resolution to allow determination of the approximate target size, burial depth, and burial angle. The combination of this information provides the necessary information regarding the presence, location, and identification of underwater UXO for effective inspection at sites requiring remedial action. Until now, there has been little or no information collected regarding the effect of seawater biofouling or corrosion on the acoustic color maps used to generate the SA features and images. This project has established that significant biofouling and/or thin corrosion layers have little impact on acoustic color or on the related classification approaches.

Conclusions

Reliable methods for accelerated production of calcareous biofouling and magnetite corrosion layers in a controlled laboratory environment have been developed for our standard munitions surrogate. Several batches of the standard munitions surrogate have undergone environmental exposure for biofouling layer development at Code 6130's site in Florida. Two inert munitions, a 155mm projectile and a 5-in rocket warhead underwent environmental exposure to develop biofouling layers. Further, the inert munitions were exposed to an accelerated production of magnetite corrosion.

EMI response data were collected for laboratory-generated and environmental exposure samples of the standard munitions surrogate. The biofouled and magnetite-corroded surrogates showed no measurable difference in the EMI response when measured in artificial sea water and when measured in air. No measurable difference was seen between bare surrogates and those with the corrosion layers applied. A small difference was observed for laboratory-generated calcareous deposits for one EMI response axis only. This result is potentially corroborated by contact, electrochemical measurements made on samples continuously exposed to seawater for a year.

The structural acoustics approach allows the formation through SAS processing of complementary three dimensional images of the sediment volume and of any targets buried therein having sufficient resolution to allow determination of the approximate target size, burial depth, and burial angle. The combination of this information provides the necessary information regarding the presence, location, and identification of underwater UXO for effective inspection at sites requiring remedial action. Until now, there has been little or no information collected regarding the effect of seawater biofouling or corrosion on the acoustic color maps used to generate the SA features and images. This project has established that significant biofouling and/or thin corrosion layers have little impact on acoustic color or on the related classification approaches.

Literature Cited

1. http://www.denix.osd.mil/uxo/EducationalResources/upload/3Rs-Maritime-Guide-2013-large.pdf

2. SanFilipo, W. and I.J. Won, 2005, "Broadband Electromagnetic Detection and Discrimination of Underwater UXO," Final Report, SERDP project MR-1321.

3. Thomas Bell, Bruce Barrow, Daniel Steinhurst, Glenn Harbaugh, Carl Friedrichs and Grace Massey, "Empirical Investigation of the Factors Influencing Marine Applications of EMI: Interim Report on Tank Testing, SERDP Project MR-2409, April 2016.

4. Shubitidze, F., "EMI Modeling for UXO Detection and Discrimination Underwater," SERDP Project MR-1632 Final Report, December 2011.

5. Hartt, W. H., Culberson, C. H., & Smith, S. W. "Calcareous Deposits on Metal Surfaces in Seawater—A Critical Review." *Corrosion*, *40*(11), 609–618 (1984).

6. De Brito, L., V. R., Coutinho, R., Cavalcanti, E. H. S., and Benchimol, M., "The influence of macrofouling on the corrosion behaviour of API 5L X65 carbon steel," *Biofouling*, *23*(3-4), 193–201 (2007).

7. Hjelt, S-E., "The Transient Electromagnetic Field of a Two-Layer Sphere," *Geoexploration*, vol. 9, 213-229 (1971).

8. Zou, Y., Wanga, J., Zhenga, Z.Z., "Electrochemical techniques for determining corrosion rate of rusted steel in seawater." Corrosion Science, Volume 53, Issue 1, January 2011, Pages 208-216.

9. Calhoun, B.A, "Magnetic and Electric Properties of Magnetite at Low Temperatures," *Phys. Rev.*, vol. 94, 1577–1585 (1954).

10. Bozorth, R.M., *Ferromagnetism*, Wiley-IEEE Press, Hoboken, 1993.

11. Gotoh, Y., Hirano, H., Nakano, M., Fujiwara, K., and Takahashi, N., "Electromagnetic Nondestructive Testing of Rust Region in Steel," IEEE Trans. Magnetics, vol. 41, 3616-3618 (2005).

12. Bucaro, J.A., Houston, B.H., Simpson, H., Calvo, D., Kraus, L., Yoder, T., Saniga, M., Dey, S., and Sarkissian, A., "Wide Area Detection and Identification of Underwater UXO Using Structural Acoustic Sensors –Final Report to SERDP MR-1513," February 2011.

13. Nelson, H.H, Bell, T., Kingdon, J., Khadr, N., and Steinhurst, D.A., "EM61-MK2 Response of Three Munitions Surrogates," NRL Memorandum Report NRL/MR/6110--090-9183, Naval Research Laboratory, Washington, DC, March 12, 2009.

14. Natishan, P.M., Jones-Meehan, J., Loeb, G.I., Little, B.J., Ray, R., and Beard, M. “Corrosion Behavior of Some Transition Metals and 4340 Steel Metals Exposed to Sulfate-Reducing Bacteria.” *Corrosion*, 55, 1062 (1999).

15. Policastro, A., Martin, F.J., Moran, P.J., and Natishan, P.M., Corrosion and Corrosion Control. Kirk-Othmer Encyclopedia of Chemical Technology, John Wiley and Sons, Inc., New York, NY (2011).

16. Kingdon, J.B., Barrow, B.J., Bell, T.H., George, D.C., Harbaugh, G.R., and Steinhurst, D.A, “TEMTADS Adjunct Sensor Systems, Hand-held EMI Sensor for Cued UXO Discrimination (ESTCP MR-200807) and Man-Portable EMI Array for UXO Detection and Discrimination (ESTCP MR-200909), Final Report,” NRL Memorandum Report NRL/MR/6110—12-9401, U.S. Naval Research Laboratory, Washington, DC, April 5, 2012.

17. Bradshaw, A. L., and Karl E. Schleicher, "Electrical conductivity of seawater," *IEEE Journal of Oceanic Engineering* 5, no. 1 (1980): 50-62.

18. Bucaro, J.A., Houston, B.H., Saniga, M., Dragonette, L.R., Yoder, T., Dey, S., Kraus, L., and Carin, L., “Broadband acoustic scattering measurements of underwater unexploded ordnance (UXO),” *J. Acoust. Soc. Am.* 123, 738-746 (2008).

19. Bucaro, J.A., Sarkissian, A., Houston, B.H., and Saniga, M., “Effects of Target Corrosion/Bio-fouling on EMI & Structural Acoustic Signatures in Underwater Environments – Acoustic Component, MR-2500” SERDP MR-2500 Final Report, June 1, 2017.